

Crystal structure of anisomycin, C<sub>14</sub>H<sub>19</sub>NO<sub>4</sub>James Kaduk<sup>1,2</sup> , Anja Dosen<sup>3</sup>  and Tom Blanton<sup>3</sup> <sup>1</sup>Department of Chemistry, Illinois Institute of Technology, 3101 South Dearborn Street, Chicago, IL 60616, USA<sup>2</sup>Department of Physics, North Central College, 131 South Loomis Street, Naperville, IL 60540, USA<sup>3</sup>International Centre for Diffraction Data (ICDD), 12 Campus Boulevard, Newtown Square, PA 19073-3273, USA

(Received 21 December 2024; revised 12 May 2025; accepted 18 May 2025)

Abstract: The crystal structure of anisomycin, C<sub>14</sub>H<sub>19</sub>NO<sub>4</sub>, has been solved and refined using synchrotron X-ray powder diffraction data, and optimized using density theory functional techniques. Anisomycin crystallizes in the space group *P*2<sub>1</sub>2<sub>1</sub>2<sub>1</sub> (#19) with *a* = 5.80382(4), *b* = 8.58149(6), *c* = 28.63508(26) Å, *V* = 1,426.183(27) Å<sup>3</sup>, and *Z* = 4 at 298 K. The crystal structure consists of layers of anisomycin molecules parallel to the *ab*-plane. The molecules form zig-zag chains of N–H⋯O and O–H⋯N hydrogen bonds along the *a*-axis. The powder pattern has been submitted to the International Centre for Diffraction Data for inclusion in the Powder Diffraction File™ (PDF®). © The Author(s), 2025. Published by Cambridge University Press on behalf of International Centre for Diffraction Data. This is an Open Access article, distributed under the terms of the Creative Commons Attribution licence (<http://creativecommons.org/licenses/by/4.0>), which permits unrestricted re-use, distribution and reproduction, provided the original article is properly cited. [doi:10.1017/S0885715625100791]

Key words: anisomycin, flagecidin, crystal structure, Rietveld refinement, density functional theory

## I. INTRODUCTION

Anisomycin (C<sub>14</sub>H<sub>19</sub>NO<sub>4</sub>, also known as flagecidin) is an antibiotic isolated from various *Streptomyces* species. It interferes with protein and DNA synthesis by inhibiting peptidyl transferase or the 80S ribosome system. Anisomycin has a role as an antiparasitic agent, a DNA synthesis inhibitor, a protein synthesis inhibitor, an antineoplastic agent, an antimicrobial agent, a bacterial metabolite, and an anticoronaviral agent (PubChem; Kim et al., 2023). The systematic name (CAS Registry No. 22862-76-6) is [(2*R*,3*S*,4*S*)-4-hydroxy-2-[(4-methoxyphenyl)methyl]pyrrolidin-3-yl] acetate. A two-dimensional molecular diagram of anisomycin is shown in Figure 1.

The crystal structure of N-acetylbromoanisomycin has been reported (Schaefer and Wheatley, 1968; CSD Refcode ANSMYC10). This structure was used to assign the stereochemistry of the parent anisomycin compound. There are 11 instances of anisomycin as a ligand in the Protein Data Bank (Berman et al., 2000), but we are unaware of any published X-ray powder diffraction data for anisomycin.

This work was carried out as part of a project (Kaduk et al., 2014) to determine the crystal structures of large-volume commercial pharmaceuticals and include high-quality powder diffraction data for them in the Powder Diffraction File™ (Kabekkodu et al., 2024).

## II. EXPERIMENTAL

Anisomycin was a commercial reagent, purchased from TargetMol (Batch #148686) and was used as received. The

white powder was packed into a 0.5-mm-diameter Kapton capillary and rotated during the measurement at ~2 Hz. The powder pattern was measured at 298(1) K at the Wiggler Low Energy Beamline (Leontowich et al. 2021) of the Brockhouse X-ray Diffraction and Scattering Sector of the Canadian Light Source using a wavelength of 0.819820(2) Å (15.1 keV) from 1.6 to 75.0° 2θ with a step size of 0.0025° and a collection time of 3 minutes. The high-resolution powder diffraction data were collected using eight Dectris Mythen2 X series 1K linear strip detectors. NIST SRM 660b LaB<sub>6</sub> was used to calibrate the instrument and refine the monochromatic wavelength used in the experiment.

The pattern was indexed using JADE Pro (MDI, 2024) on a primitive orthorhombic unit cell with *a* = 5.80213, *b* = 8.58159, *c* = 28.64755 Å, *V* = 1,426.41 Å<sup>3</sup>, and *Z* = 4. The suggested space group was *P*2<sub>1</sub>2<sub>1</sub>2<sub>1</sub>, which was confirmed by the successful solution and refinement of the structure. A reduced cell search of the Cambridge Structural Database (Groom et al., 2016), with the chemistry H, C, N, and O only, yielded 31 hits, but no structures for anisomycin or its derivatives.

The crystal structure was solved by direct methods as implemented in EXPO2014 (Altomare et al., 2013). All of the non-H atoms were assigned correctly. The opposite enantiomer to that indicated by PubChem (Kim et al., 2023) was obtained, so the structure was inverted using Mercury (Macrae et al., 2020), and the hydrogen atoms were added.

Rietveld refinement was carried out with GSAS-II (Toby and Von Dreele, 2013). Only the 3.0–50.0° portion of the pattern was included in the refinements (*d*<sub>min</sub> = 0.970 Å). All non-H-bond distances and angles were subjected to restraints, based on a Mercury/Mogul Geometry Check

Corresponding author: James Kaduk; Email: [kaduk@polycrystallography.com](mailto:kaduk@polycrystallography.com)



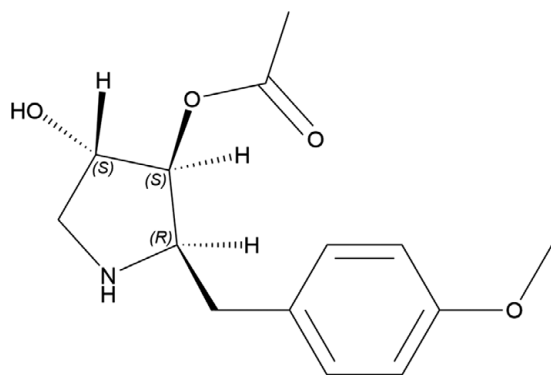


Figure 1. The two-dimensional structure of anisomycin.

(Bruno et al., 2004; Sykes et al., 2011). The Mogul average and standard deviation for each quantity were used as the restraint parameters. The phenyl ring was restrained to be planar. The restraints contributed 1.6% to the overall  $\chi^2$ . The hydrogen atoms were included in calculated positions, which were recalculated during the refinement using Materials Studio (Dassault Systèmes, 2023). The  $U_{\text{iso}}$  of the heavy atoms were grouped by chemical similarity. The  $U_{\text{iso}}$  of the H atoms were fixed at  $1.3 \times$  the  $U_{\text{iso}}$  of the heavy atoms to which they are attached. The peak profiles were described using the generalized (Stephens, 1999) microstrain model. The background was modeled using a six-term shifted Chebyshev polynomial, with a peak at  $10.54^\circ$  to model the scattering from the Kapton capillary and any amorphous component.

The final refinement of 84 variables using 18,401 observations and 48 restraints yielded the residual  $R_{\text{wp}} = 0.05776$ . The largest peak ( $1.68 \text{ \AA}$  from C5) and hole ( $1.93 \text{ \AA}$  from O4) in the difference Fourier map were  $0.47(11)$  and  $-0.45(11) \text{ e\AA}^{-3}$ , respectively. The final Rietveld plot is shown in

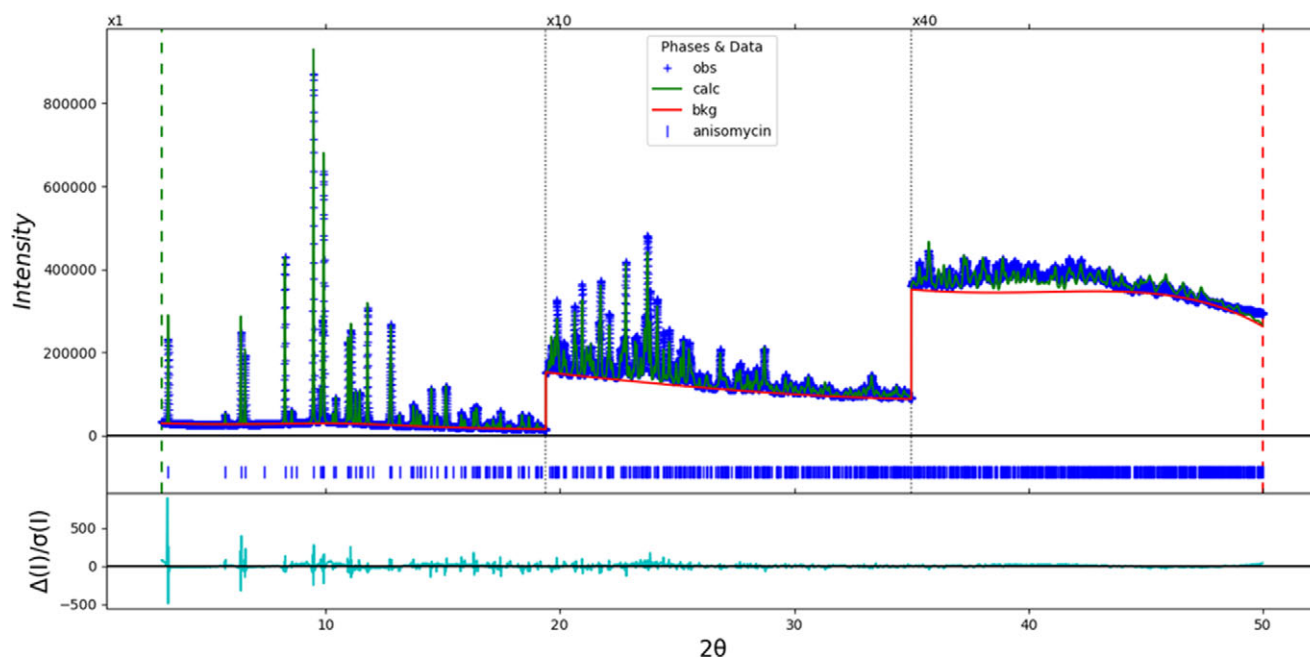


Figure 2. The Rietveld plot for anisomycin. The blue crosses represent the observed data points, and the green line represents the calculated pattern. The cyan curve indicates the normalized error plot, and the red line indicates the background curve. The vertical scale has been multiplied by a factor of  $10 \times$  for  $2\theta > 19.4^\circ$  and by a factor of  $40 \times$  for  $2\theta > 35.0^\circ$ .

Figure 2. The largest features in the normalized error plot are in the shapes of some of the strong low-angle peaks. These misfits probably indicate subtle changes in the specimen during the measurement.

The crystal structure of anisomycin was optimized (fixed experimental unit cell) with density functional theory techniques using VASP (Kresse and Furthmüller, 1996) through the MedeA graphical interface (Materials Design, 2024). The calculation was carried out on 32 cores of a 144-core (768-GB memory) HPE Superdome Flex 280 Linux server at North Central College. The calculation used the GGA-PBE functional, a plane wave cutoff energy of 400.0 eV, and a  $k$ -point spacing of  $0.5 \text{ \AA}^{-1}$ , leading to a  $3 \times 2 \times 1$  mesh, and took  $\sim 3.6$  hours. Single-point density functional calculations (fixed experimental cell) and population analysis were carried out using CRYSTAL23 (Erba et al., 2023). The basis sets for the H, C, N, and O atoms in the calculation were those of Gatti et al. (1994). The calculations were run on a 3.5-GHz PC using eight  $k$ -points and the B3LYP functional and took  $\sim 1.5$  hours.

### III. RESULTS AND DISCUSSION

The root-mean-square (rms) Cartesian displacement of the non-H atoms in the Rietveld-refined and VASP-optimized molecules is  $0.111 \text{ \AA}$  (Figure 3); the largest difference is  $0.288 \text{ \AA}$  at O3. The agreement is within the normal range for correct structures (van de Streek and Neumann, 2014). The asymmetric unit is illustrated in Figure 4. The remaining discussion will emphasize the VASP-optimized structure.

All of the bond distances, bond angles, and torsion angles fall within the normal ranges indicated by a Mercury Mogul Geometry check (Macrae et al., 2020). The anisomycin of this study and the previously mentioned N-acetylbromoanisomycin molecules have different conformations (Figure 5), but all of the torsion angles fall within the normal ranges. Quantum chemical

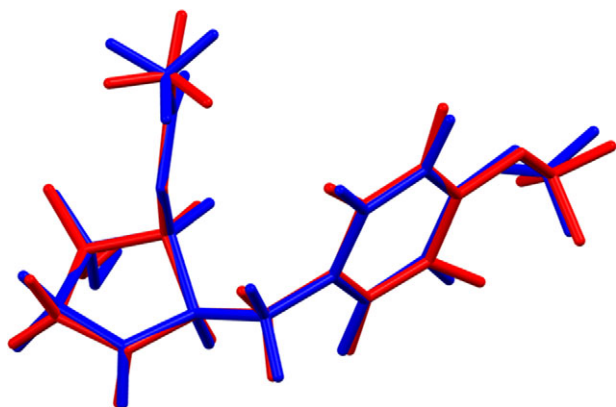


Figure 3. Comparison of the Rietveld-refined (red) and VASP-optimized (blue) structures of anisomycin. The root-mean-square Cartesian displacement is 0.111 Å. Image generated using Mercury (Macrae et al., 2020).

geometry optimization of the isolated anisomycin molecule (DFT/B3LYP/6-31G\*/water) using Spartan '24 (Wavefunction, Inc., 2023) indicated that the observed conformation is 4.3 kcal/mol higher in energy than a local minimum, but very similar in geometry (rms Cartesian displacement = 0.268 Å). The global minimum-energy conformation is very similar.

The crystal structure (Figure 6) consists of layers of anisomycin molecules parallel to the *ab*-plane. The molecules form hydrogen-bonded chains along the *a*-axis. The mean plane of the phenyl ring is approximately (5, 7, 19). The Mercury Aromatics Analyser indicates a moderate interaction, with a minimum ring–ring distance of 5.8 Å.

Analysis of the contributions to the total crystal energy of the structure using the Forcite module of Materials Studio (Dassault Systèmes, 2023) indicates that bond, angle, and torsion distortion terms contribute significantly to the intramolecular energy. The intermolecular energy is dominated by electrostatic attractions, which, in this force field-based analysis, also include hydrogen bonds. The hydrogen bonds

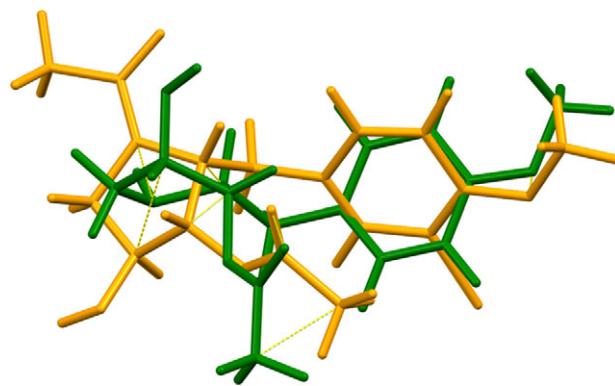


Figure 5. Comparison of the molecular structures of anisomycin (green) and N-acetylbromoanisomycin (orange).

are better discussed using the results of the density functional theory (DFT) calculation.

There are two classical hydrogen bonds in the structure (Table I), between the hydroxyl group O3 and the amino group N1. These form zig-zag chains along the *c*-axis (Figure 7). The energy of the N–H...O hydrogen bond was calculated using the correlation of Wheatley and Kaduk (2019). Several C–H...O hydrogen bonds also contribute to the lattice energy.

The volume enclosed by the Hirshfeld surface of anisomycin (Figure 8; Hirshfeld, 1977; Spackman et al., 2021) is 350.09 Å<sup>3</sup>, 98.19% of half the unit cell volume. The packing density is, thus, looser than normal. The only significant close contacts (red in Figure 8) involve the hydrogen bonds. The volume/non-hydrogen atom is higher than normal at 18.8 Å<sup>3</sup>.

The Bravais–Friedel–Donnay–Harker (Bravais, 1866; Friedel, 1907; Donnay and Harker, 1937) algorithm suggests that we might expect platy morphology for anisomycin, with {001} as the principal faces. A second-order spherical harmonic model was included in the refinement. The texture index was 1.012(0), indicating that the preferred orientation was not significant in this rotated capillary specimen.

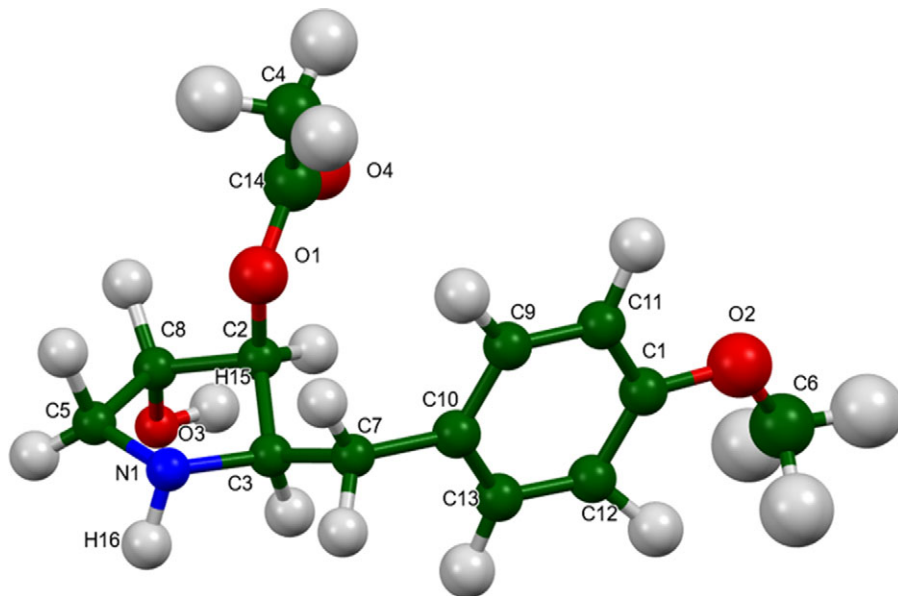


Figure 4. The asymmetric unit of anisomycin, with the atom numbering. The atoms are represented by 50% probability spheroids. Image generated using Mercury (Macrae et al., 2020).

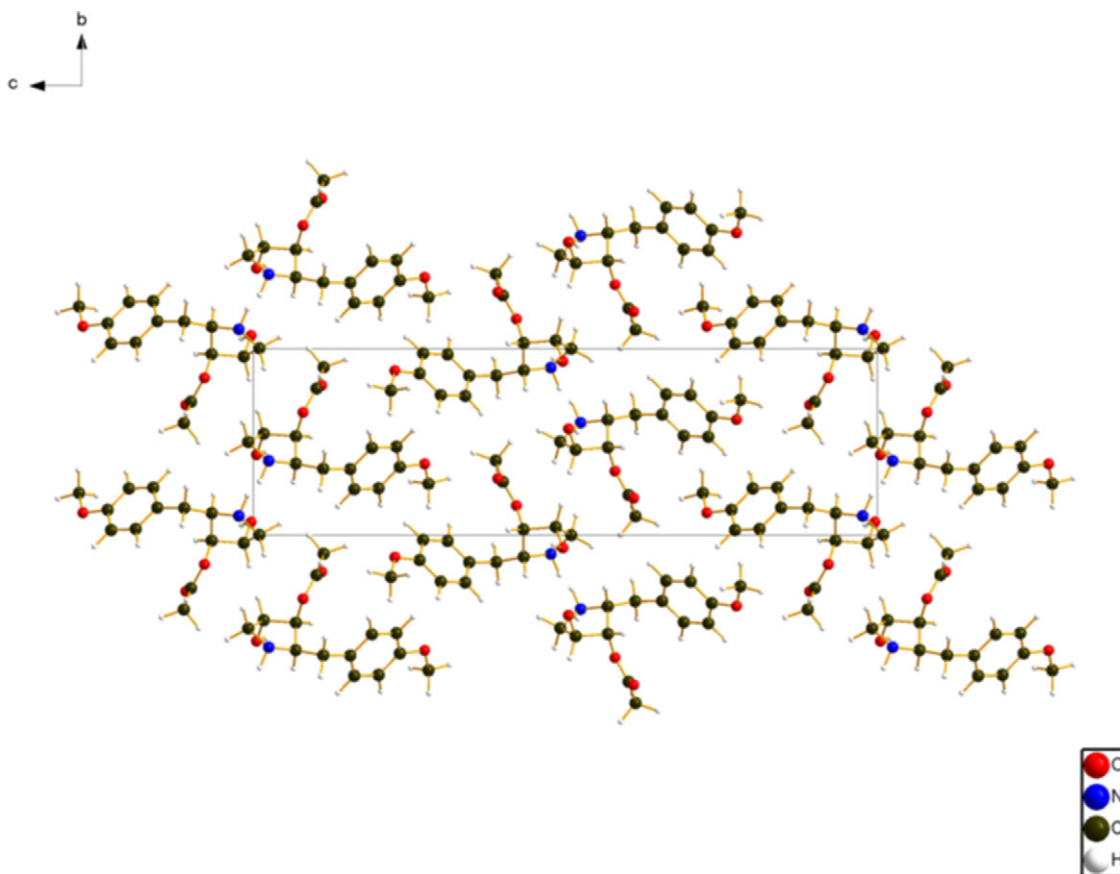


Figure 6. The crystal structure of anisomycin, viewed down the  $a$ -axis. Image generated using Diamond (Crystal Impact, 2023).

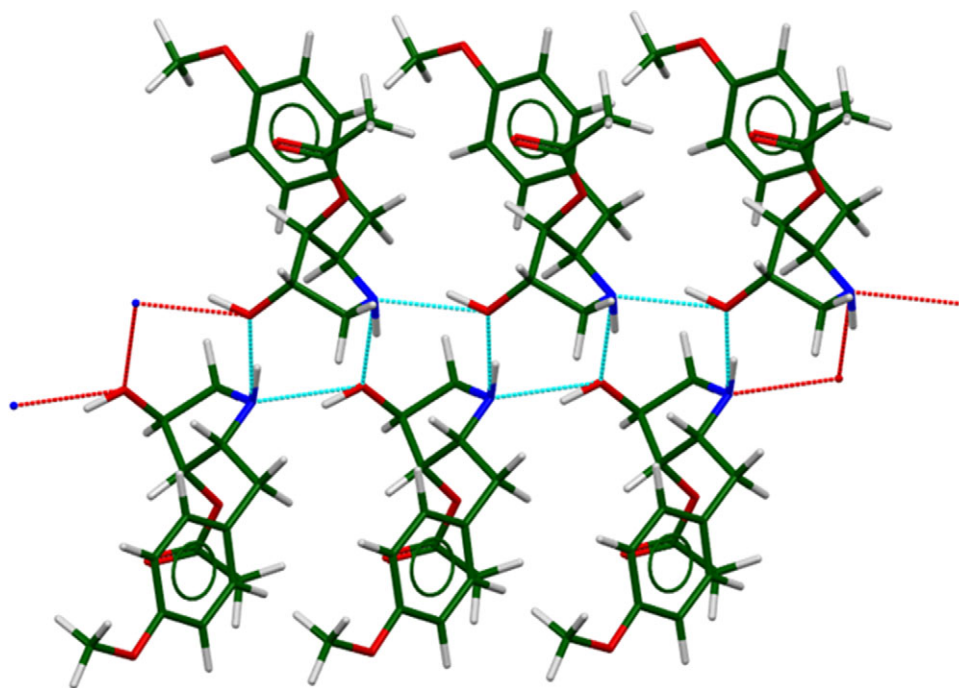


Figure 7. The hydrogen-bonded chains in anisomycin. Image generated using Mercury (Macrae et al., 2020). The cyan dashed lines are hydrogen bonds within a single asymmetric unit, and the red lines are those between asymmetric units. The  $c$ -axis is horizontal, the  $a$ -axis is vertical, and the view is down the  $b$ -axis.

TABLE I. Hydrogen bonds (CRYSTAL23) in anisomycin

H-bond	D–H, Å	H…A, Å	D…A, Å	D–H…A, °	Mulliken overlap, <i>e</i>	<i>E</i> , kcal/mol
O3–H15…N1	1.010	1.876	2.800	150.6	0.080	
N1–H16…O3	1.031	1.932	2.935	163.3	0.056	5.5
C2–H17…O4	1.097	2.400 <sup>a</sup>	2.743	96.1	0.015	
C4–H20…O3	1.101	2.724	3.642	140.7	0.014	
C4–H21…O4	1.096	2.558	3.625	164.1	0.013	
C6–H24…O4	1.094	2.322	3.388	164.0	0.021	
C12–H32…O2	1.090	2.786	3.821	158.4	0.013	

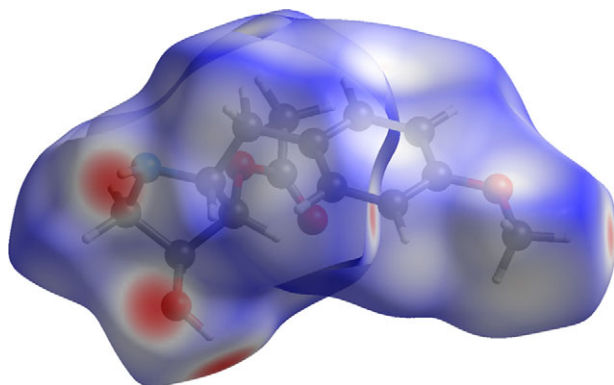
<sup>a</sup>Intramolecular.

Figure 8. The Hirshfeld surface of anisomycin. Intermolecular contacts longer than the sums of the van der Waals radii are colored blue, and contacts shorter than the sums of the radii are colored red. Contacts equal to the sums of radii are white. Image generated using CrystalExplorer (Spackman et al., 2021).

## ACKNOWLEDGEMENTS

We thank Adam Leontowich for his assistance in the data collection.

## DATA AVAILABILITY STATEMENT

The powder pattern of anisomycin from this synchrotron dataset has been submitted to the International Centre for Diffraction Data (ICDD) for inclusion in the Powder Diffraction File. The Crystallographic Information Framework (CIF) files containing the results of the Rietveld refinement (including the raw data) and the DFT geometry optimization were deposited with the ICDD. The data can be requested at [pdj@icdd.com](mailto:pdj@icdd.com).

## FUNDING STATEMENT

Part or all of the research described in this paper was performed at the Canadian Light Source, a national research facility of the University of Saskatchewan, which is supported by the Canada Foundation for Innovation (CFI), the Natural Sciences and Engineering Research Council (NSERC), the Canadian Institute of Health Research (CIHR), the Government of Saskatchewan, and the University of Saskatchewan. This work was partially supported by the International Centre for Diffraction Data.

## CONFLICTS OF INTEREST

The authors have no conflicts of interest to declare.

## REFERENCES

- Altomare, A., C. Cuocci, C. Giacovazzo, A. Moliterni, R. Rizzi, N. Corriero, and A. Falcicchio. 2013. "EXPO2013: A Kit of Tools for Phasing Crystal Structures from Powder Data." *Journal of Applied Crystallography* 46: 1231–35.
- Berman, H. M., J. Westbrook, Z. Feng, G. Gilliland, T. N. Bhat, H. Weissig, I. N. Shindyalov, and P. E. Bourne. 2000. "The Protein Data Bank." *Nucleic Acids Research* 28: 235–42. <https://doi.org/10.1093/nar/28.1.235>; rcsb.org.
- Bravais, A. 1866. *Etudes Cristallographiques*. Gauthier Villars.
- Bruno, I. J., J. C. Cole, M. Kessler, J. Luo, W. D. S. Motherwell, L. H. Purkis, B. R. Smith, et al. 2004. "Retrieval of Crystallographically Derived Molecular Geometry Information." *Journal of Chemical Information and Computer Sciences* 44: 2133–44.
- Crystal Impact. 2023. *Diamond V. 5.0.0*. Crystal Impact – Dr. H. Putz & Dr. K. Brandenburg.
- Dassault Systèmes. 2023. *BIOVIA Materials Studio 2024*. BIOVIA.
- Donnay, J. D. H., and D. Harker. 1937. "A New Law of Crystal Morphology Extending the Law of Bravais." *American Mineralogist* 22: 446–67.
- Erba, A., J. K. Desmarais, S. Casassa, B. Civalieri, L. Donà, I. J. Bush, B. Searle, et al. 2023. "CRYSTAL23: A Program for Computational Solid State Physics and Chemistry." *Journal of Chemical Theory and Computation* 19: 6891–932. <https://doi.org/10.1021/acs.jctc.2c00958>.
- Friedel, G. 1907. "Etudes sur la loi de Bravais." *Bulletin de la Société Française de Minéralogie* 30: 326–455.
- Gatti, C., V. R. Saunders, and C. Roetti. 1994. "Crystal-Field Effects on the Topological Properties of the Electron-Density in Molecular Crystals – the Case of Urea." *Journal of Chemical Physics* 101: 10686–96.
- Groom, C. R., I. J. Bruno, M. P. Lightfoot, and S. C. Ward. 2016. "The Cambridge Structural Database." *Acta Crystallographica Section B: Structural Science, Crystal Engineering and Materials* 72: 171–79.
- Hirshfeld, F. L. 1977. "Bonded-Atom Fragments for Describing Molecular Charge Densities." *Theoretica Chimica Acta* 44: 129–38.
- Kabekkodu, S., A. Dosen, and T. N. Blanton. 2024. "PDF-5+: A Comprehensive Powder Diffraction File™ for Materials Characterization." *Powder Diffraction* 39: 47–59.
- Kaduk, J. A., C. E. Crowder, K. Zhong, T. G. Fawcett, and M. R. Suchomel. 2014. "Crystal Structure of Atomoxetine Hydrochloride (Strattera), C<sub>17</sub>H<sub>22</sub>NOCl." *Powder Diffraction* 29: 269–73.
- Kim S., J. Chen, T. Cheng, A. Gindulyte, J. He, S. He, Q. Li, et al. 2023. "PubChem 2023 update." *Nucleic Acids Research* 51 (D1): D1373–80. <https://doi.org/10.1093/nar/gkac956>.
- Kresse, G., and J. Furthmüller. 1996. "Efficiency of Ab-Initio Total Energy Calculations for Metals and Semiconductors Using a Plane-Wave Basis Set." *Computational Materials Science* 6: 15–50.
- Leontowich, A. F. G., A. Gomez, B. Diaz Moreno, D. Muir, D. Spasyuk, G. King, J. W. Reid, C.-Y. Kim and S. Kycia. 2021. "The lower energy diffraction and scattering side-bounce beamline for materials science at the Canadian Light Source." *Journal of Synchrotron Radiation* 28: 961–969.
- Macrae, C. F., I. Sovago, S. J. Cottrell, P. T. A. Galek, P. McCabe, E. Pidcock, M. Platings, et al. 2020. "Mercury 4.0: From Visualization to Design and Prediction." *Journal of Applied Crystallography* 53: 226–35.
- Materials Design. 2024. *MedeA 3.7.2*. Materials Design, Inc.
- MDI. 2024. *JADE Pro Version 9.0*. Materials Data.

- Schaefer, J. P., and P. J. Wheatley. 1968. "Structure of Anisomycin." *Journal of Organic Chemistry* 33: 166–69. <https://doi.org/10.1021/jo01265a031>.
- Spackman, P. R., M. J. Turner, J. J. McKinnon, S. K. Wolff, D. J. Grimwood, D. Jayatilaka, and M. A. Spackman. 2021. "CrystalExplorer: A Program for Hirshfeld Surface Analysis, Visualization and Quantitative Analysis of Molecular Crystals." *Journal of Applied Crystallography* 54: 1006–11. <https://doi.org/10.1107/S1600576721002910>; <https://crystalexplorer.net>.
- Stephens, P. W. 1999. "Phenomenological Model of Anisotropic Peak Broadening in Powder Diffraction." *Journal of Applied Crystallography* 32: 281–89.
- Sykes, R. A., P. McCabe, F. H. Allen, G. M. Battle, I. J. Bruno, and P. A. Wood. 2011. "New Software for Statistical Analysis of Cambridge Structural Database Data." *Journal of Applied Crystallography* 44: 882–86.
- Toby, B. H., and R. B. Von Dreele. 2013. "GSAS II: The Genesis of a Modern Open Source All Purpose Crystallography Software Package." *Journal of Applied Crystallography* 46: 544–49.
- van de Streek, J., and M. A. Neumann. 2014. "Validation of Molecular Crystal Structures from Powder Diffraction Data with Dispersion-Corrected Density Functional Theory (DFT-D)." *Acta Crystallographica Section B: Structural Science, Crystal Engineering and Materials* 70: 1020–32.
- Wavefunction, Inc. 2023. *Spartan '24. V. 1.0.0*. Wavefunction, Inc.
- Wheatley, A. M., and J. A. Kaduk. 2019. "Crystal Structures of Ammonium Citrates." *Powder Diffraction* 34: 35–43.